# Optimization Method for Systematically Improving Non-contact R-test Accuracy

Lei Jiang[1], Bingkang Peng[1], Guofu Ding[1], Shengfeng Qin[2], Jian Zhang[1*], Yong Li[1]

1. Institute of Advanced Design and Manufacturing, School of Mechanical Engineering, Southwest Jiaotong University, Sichuan Chengdu 610031, China

2. School of Design, Northumbria University, Newcastle upon Tyne NE1 8ST, UK

Abstract: Non-contact R-test is an instrument to measure the synchronous errors of five-axis machine tools. However, there are still some deficiencies in its researches, such as the difficult and laborious calibrations. How to systematically improve the measurement accuracy with a good balance to minimum cost is a real problem in guiding practice. This paper proposes a new systematic optimization method to solve this problem based on comprehensive understanding of the non-contact R-test in terms of structure parameters and relations. Firstly, the algorithm for sphere center coordinates is established based on the self-adaptive differential evolution algorithm to obtain the definite computational accuracy and efficiency. Secondly, the parameters of the fixture structure are optimized to maximize the measurement stability, measuring space and noninterference space. Thirdly, the on-machine calibration is performed to replace pre-calibration and re-calibration, and to establish the positional relationships between sensors, the fixture and the machine tool simultaneously. It can reduce the difficulties of manufacture, maintenance and application. Fourthly, the measurement accuracy can be evaluated to determine whether the iterative optimization achieves the goal. The proposed method has been verified with case studies to support optimized non-contact R-test setting up, leading to cost-effective and accuracy test on five-axis machine tools.

**Keywords:** optimization method; non-contact R-test; structural parameter; on-machine calibration; measurement accuracy.

## 1 Introduction

With the rising on machining accuracy, more measurement requirements for five-axis machine tools are put forward, such as the dynamic synchronous errors analysis of simultaneous multi-axis interpolation. In recent years, a type of special instrument - R-test has been developed. The R-test can measure 3D displacement of a precision sphere attached to spindle relative to a fixture(“sensors nest”[1]) fixed on worktable by using three displacement sensors[2]. Similar to the application of double ball-bar (DBB), the sphere can rotate and move relative to the fixture without affecting their positional relationship. Weikert firstly introduced R-Test as an instrument for accuracy measurement on five-axis machine tools[3]. The R-test is described in ISO 230-1:2012 (Clause 11.3.5.3)[4]. The inclusion of R-test application to dynamic measurement of synchronization errors of a rotary axis to linear axes has been discussed in

* Jian Zhang is corresponding author: jerrysmail@263.net

ISO/TC39/SC2[4]. It can identify the location errors of the rotary axis by static test based on ISO 230-7[5], and the synchronous errors of circular interpolation by dynamic test based on ISO 10791-6[1][6][7][8].

Compared with DBB, R-test has better measurement efficiency and data correspondence (3D relative positional change of sphere). It has been applied in the field of inspection and error calibration for five-axis machine tools. IBS Precision Engineering[9][10], FIDIA[11] and other companies have produced different types of R-test.

According to the classification of displacement sensors, the R-test can be divided into two types: contact or non-contact. Related research and application mainly focus on the contact one. Liu et al. proposed two indicators (measuring space and measurement stability) for evaluating the performance and a structure optimization method for contact R-test[8]. Li et al. deduced conversion matrix between the sensor reading and the 3D relative positional change of sphere, and the main error factors affecting the measurement accuracy were determined[12]. Bringmann et al. established the motion and error model of the rotary axis of five-axis machine tools, and the error identification based on contact R-test was carried out[13]. Hong et al. presented an efficient and automated scheme to observe error motions of rotary axes on a five-axis machine tool by contact R-test[14]. Ibaraki et al. applied contact R-test to measure four geometric errors of the rotary axis by some specific tool path[15]. Lei et al. applied contact R-test to research dynamic accuracy evaluation for five-axis machine tools by testing S trajectory deviation[1].

In general, contact R-test has advantages on simplicity and reliability, but its accuracy may be influenced by friction, abrasion, deformation and dynamics of the sensors in some applications. The influence of friction or supporting spring may be significant due to varied measurement conditions (e.g. feedrate, material property of sphere or contact surface). This in turn may cause measurement error up to about 6 μm and response delay in high frequency dynamic test[2]. In addition, a critical issue is the crash caused by mis-programming[2].

With the increasing measurement demand for dynamic performance on five-axis machine tools, non-contact R-test has been attracted more and more attention. Relative to contact R-test, non-contact R-test has some potentially significant advantages [2][16][17]:

(1) It is not influenced at all by the friction and dirt on sphere and sensor, but it measures with better stability and accuracy retention.

(2) It is not influenced at all by the dynamics of supporting spring, but can analyze the characters of high frequency dynamic responses.

(3) It is safe due to long distance between the sphere and sensors with better convenience.

(4) It can be applied to evaluate parameters of spindle based on ISO 203-7, ISO/TR 17243-2 when the spindle speed range is 600 - 30,000 RPM[10][18].

Hong et al. developed a non-contact R-test with laser displacement sensor to prove its advantage[2]. Li et al. proposed a method for identifying geometric errors for the rotary axis of five-axis machine tools with non-contact R-test[19]. Florissant and Spaan proposed some dynamic test methods for five-axis machine tools based on non-contact R-test[20][21][22]. However, there are still some deficiencies in the research of non-contact R-test:

(1) The accuracy of the non-contact R-test depends largely on the expensive non-contact displacement sensor, such as laser or eddy current displacement sensor.

(2) The structure of the non-contact R-test is more complicated, and the debugging is difficult.

(3) The calibrations (including pre-calibration by manufacturer and re-calibration by user) are difficult and laborious. Even with high precision pre-calibration, the measurement accuracy is influenced to a great degree by re-calibration.

(4) For real-time dynamic testing, the computational accuracy and efficiency are difficult to meet at the same time.

(5) In addition to measurement accuracy, other aspects (e.g. measurement stability, measuring space and noninterference space) should be paid more attention.

Therefore, it is necessary and important in practice to develop an optimal setting-up method for non-contact R-test for easy manufacture, maintenance and application meanwhile systematically promising expected measurement accuracy with minimum cost. However, how to set up correctly and conveniently is little reported. Therefore, the following factors should be taken into account:

(1) The eccentricity of sphere center from the line representing sensor sensitive direction introduces an error for calculating sphere coordinates when the conventional algorithm for contact R-test is applied[23].

(2) The parameters of the fixture structure need to be optimized according to the different types of sensor and its measurement performance.

(3) The relative position between the sphere, fixture and machine tool should be calibrated at the same time.

(4) Maximize the advantages of non-contact sensor to reduce the cost and improve the measurement accuracy.

This paper proposes a systematic optimization method for setting-up of non-contact R-test with a goal of achieving better measurement accuracy. The contributions of this paper are follows:

(1) The self-adaptive differential evolution (SADE) algorithm is applied to calculate the sphere center coordinates, which can obtain the definite computational accuracy and efficiency.

(2) The parameters optimization of the fixture structure can maximize measurement stability, measuring space and noninterference space.

(3) The on-machine calibration replaces pre-calibration and re-calibration to establish the positional relationships among the sensors, the fixture and the machine tool simultaneously. It can reduce the difficulties of manufacture, maintenance and application.

(4) The measurement accuracy can be evaluated to determine whether the optimization achieves the goal.

The rest of the paper is organized as follows. In section 2, the exploration of the optimization problem spaces and variable spaces is conducted based on the comprehensive understanding of the non-contact R-test principle. In section 3, the systematic optimization method for setting-up the non-contact R-test is detailed. In section 4, the case study tests on the proposed method are presented and discussed. Finally, some conclusions are drawn in section 5.

## 2 Understanding of non-contact R-test

The correct understanding of non-contact R-test is a prerequisite for establishing a systematic optimization method for high measurement accuracy by exploring its problem spaces (goals and constraints) and variable spaces (controls). Typical structure of a non-contact R-test is shown in Fig.1. Three sensors are annularly distributed around the sphere to avoid collision with the sphere. Define the circular plane at the end of sensor $i$ ($i$=1, 2, 3) as a probe plane $i$, which is perpendicular to the sensor axis. The sensor can measure the distance between the sphere center and probe plane. Before test, the sphere center should be aligned with the spindle axis, which can be realized by monolithic tool holder or special adjustable alignment holder[9].

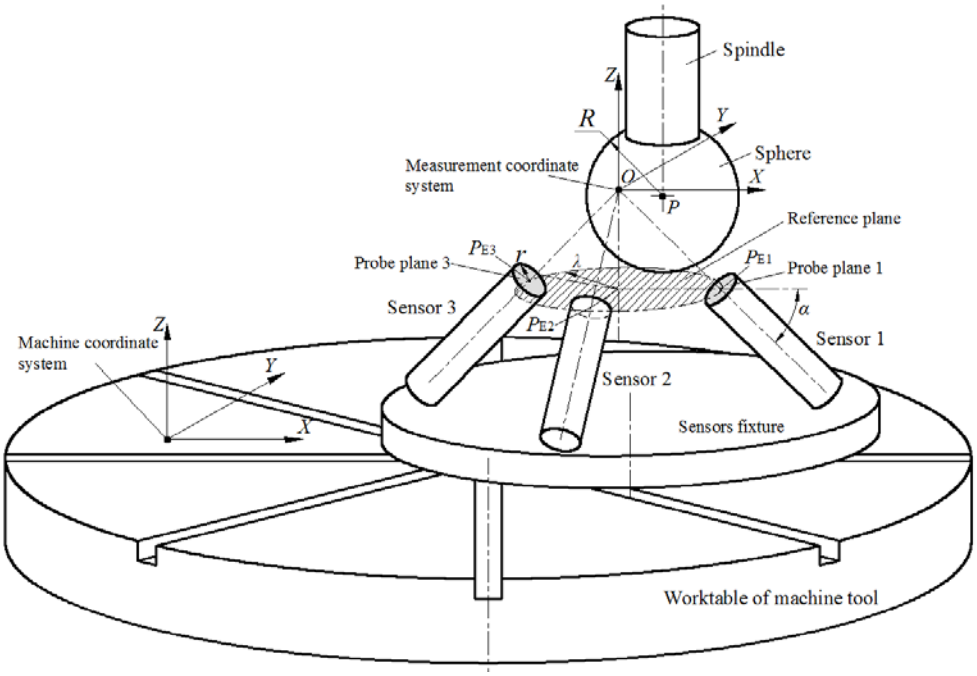


Fig.1 The structure diagram of non-contact R-test.

Define the sphere center as $P(x, y, z)$, the center of probe plane $i$ as $P_{Ei}(x_{Ei}, y_{Ei}, z_{Ei})$, the plane surrounded by $P_{Ei}$ as reference plane, the radius of sphere as $R$, the radius of probe plane as $r$, the tilt angle between the sensor axis and the reference plane as $\alpha$ ($0<\alpha<90°$), and the contour radius of the reference plane as $\lambda$.

The data measured by the sensors can be converted to the displacement of the sphere center in X/Y/Z directions in the measurement coordinate system (MCS) which are parallel to the corresponding directions of the machine coordinate system. To simplify the calculation, the reference plane could be set to be parallel to the XOY coordinate plane of MCS, and the origin is set to the intersection of sensors axes theoretically.

Define the distance between probe plane $i$ and sphere surface/center as $l_i$ / $L_i$ respectively, the distance between axis $i$ and the sphere center as $r_i$. The spatial relationship between the sensor and the sphere is shown in Fig.2.

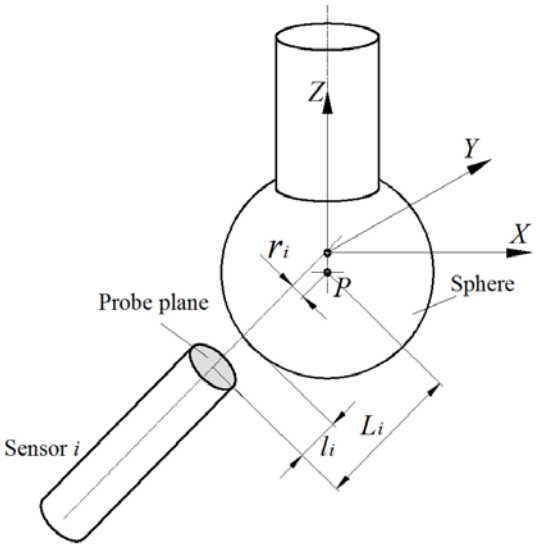


Fig.2 The spatial relationship between the sensor and sphere.

The displacement of the sphere center can be applied to identify the synchronous errors of simultaneous multi-axis interpolation and location errors of the rotary axis. Now the problem is how to select the sensor and sphere, to set up and adjust geometric parameters of the fixture and to install the fixture on the worktable in a cost-effective way. The goal is to achieve expected measurement accuracy within minimum cost. The design variables (controls) are as follows:

(1) Parameters of non-contact displacement sensor relating to cost, measurement accuracy and capability.

(2) Parameters of the fixture structure relating to measurement stability and capability.

(3) Calibration of R-test relating to measurement accuracy and the cost of manufacture, maintenance and use.

# 3 Systematic optimization method

## 3.1 The overview of the systematic optimization method

In the proposed optimization process (See Fig. 3), the calculation for the sphere center coordinates is a starting point for optimization. Following this up, the parameters of the sphere and the sensor are determined/chosen. Then, the optimization of the fixture structure is performed in connection to the on-machine calibration and the prediction of uncertainty, when an on-machine predicted cost-effective measurement accuracy is obtained, the optimization process will be terminated; otherwise, the process will go back to adjust the parameters of the sensor and the sphere in an iterative fashion until the optimization process is completed.

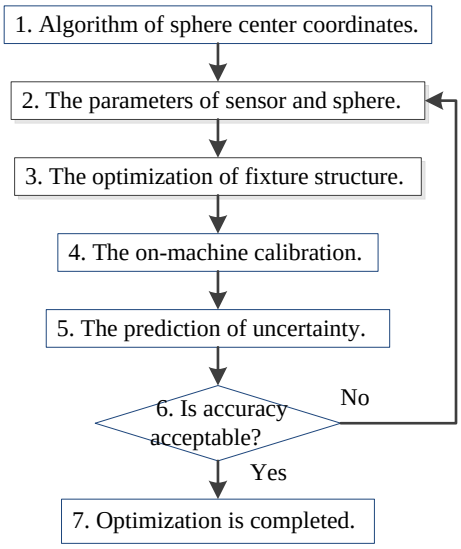


Fig.3 The flowchart of the proposed systematic optimization method.

## 3.2 The algorithm for computing the sphere center coordinates

The probe plane based on MCS can be expressed as follows:

$$\begin{cases} a_i x + b_i y + c_i z + d_i = 0 \\ a_i^2 + b_i^2 + c_i^2 = 1 \end{cases}, \quad (i = 1,2,3), \tag{1}$$

where $a_i$, $b_i$, $c_i$, $d_i$ are the equation parameters of probe plane $i$.

According to the distance between $P$ and the probe plane (see Fig. 2), the geometric positional relationship between the $P$ and $P_{Ei}$ can be expressed by the following equations:

$$\begin{cases} (x - x_{Ei})^2 + (y - y_{Ei})^2 + (z - z_{Ei})^2 = r_i^2 + L_i^2, \\ L_i = |a_i x + b_i y + c_i z + d_i|, \\ R + l_{\min} \le L_i \le R + l_{\min} + \delta, \\ 0 \le r_i \le r_{\max}, \end{cases} \quad (i = 1,2,3) \ . \tag{2}$$

By solving the Eq. (2), the coordinates of the point $P$ can be obtained. However, the solution cannot be obtained by theoretical formulas directly because of measurement errors. So the numerical method for solving an optimization problem is adopted. Define the relationship function as follows:

$$f_i(x,y,z) = (x - x_{Ei})^2 + (y - y_{Ei})^2 + (z - z_{Ei})^2 - r_i^2 - L_i^2 = 0, \quad (i = 1,2,3). \tag{3}$$

According to the Eq. (3), the objective function can be expressed as the Eq. (4)

$$G(x,y,z) = \sum_{i=1}^{3} f_i^2(x,y,z), \quad (i = 1,2,3). \tag{4}$$

The closer the value of $G$ to zero is, the more accurate the solution is. Compared with traditional solution algorithms, the SADE algorithm has been adopted for its characteristics of high computational efficiency and robustness[24]. By setting the self-adaptive variation operator and crossover operator, it can avoid low search efficiency and poor global optimal solutions [24][25][26].

Based on ISO 230-7 and ISO10791-6, the accuracy tests of five-axis machine tools are divided into static

and dynamic types. Static test is intermittent measurement for multi-axis positioning errors. It can identify squareness and offset of the rotary axis. Dynamic test is continuous measurement with simultaneous multi-axis interpolation. It can analyze performances of the machine controller, such as servo mismatch, reversal peak and dynamic compliance, etc.

For static test, the focus is on the solution accuracy. While for dynamic test, the focus is on the solution accuracy and computational efficiency. Tab.1 shows the parameters of SADE algorithm in different test modes. (The SADE algorithm is compiled with VC++, the CPU of computer is Celeron 2.8G.).

Tab.1 The parameters of SADE algorithm in two test modes.

| Test modes | Number of Population | Number of generation | Error of solution | Solution time |
|---|---|---|---|---|
| Static test | 30 | 300 | <0.1 μm | <0.015 s |
| Dynamic test | 20 | 200 | < 0.2 μm | <0.001 s |

Based on the SADE algorithm, the computing results can meet the general requirements about the measurement accuracy and sampling frequency. If hardware is upgraded, the efficiency can be improved further.

## 3.3 The parameters optimization of the fixture structure

In addition to measurement accuracy, the performances of non-contact R-test include measurement stability, measuring space and noninterference space[8]. The measurement stability refers to the definite relation between the coordinates of the sphere and the distances between the sensors and sphere. The measuring space is the range in which the sphere center can be moved during test. The noninterference space is the range in which the sphere can be moved without collision with the probe planes. For the definite sphere and sensor, the adjustable parameters of the fixture structural are the tilt angle $\alpha$ and contour radius $\lambda$. The above performances could be achieved by optimizing the two parameters.

### 3.3.1 The optimization of the tilt angle

Tilt angle $\alpha$ is related to maximum measurement stability. By the Eq. (2), $L_i$ can be expressed as follows:

$$\begin{bmatrix} L_1 \\ L_2 \\ L_3 \end{bmatrix} = \begin{bmatrix} a_1 & b_1 & c_1 \\ a_2 & b_2 & c_2 \\ a_3 & b_3 & c_3 \end{bmatrix} \cdot \begin{bmatrix} x \\ y \\ z \end{bmatrix}. \tag{5}$$

Without loss of generality, suppose the axis of sensor 1 to be located in the XOZ coordinate plane of MCS. According to the unit vector of each sensor axis, the Eq. (5) can be rewritten as follows:

$$\begin{bmatrix} L_1 \\ L_2 \\ L_3 \end{bmatrix} = \begin{bmatrix} -\cos\alpha & 0 & \sin\alpha \\ \cos\alpha \cdot \sin 30° & \cos\alpha \cdot \cos 30° & \sin\alpha \\ \cos\alpha \cdot \sin 30° & -\cos\alpha \cdot \cos 30° & \sin\alpha \end{bmatrix} \cdot \begin{bmatrix} x \\ y \\ z \end{bmatrix} = \boldsymbol{J} \cdot \begin{bmatrix} x \\ y \\ z \end{bmatrix}, \tag{6}$$

where matrix $\boldsymbol{J}$ indicates the relationship between the coordinates of the sphere center and $L_{i\text{-}j}$.

The stability can be evaluated by the condition number of matrix $\boldsymbol{J}$. The smaller the condition number is, the better the stability is. The relationship between the condition number and the tilt angle is shown in Fig.4. When the tilt angle is about 35.27° (each sensor is perpendicular to each other), the stability reaches its

maximum.

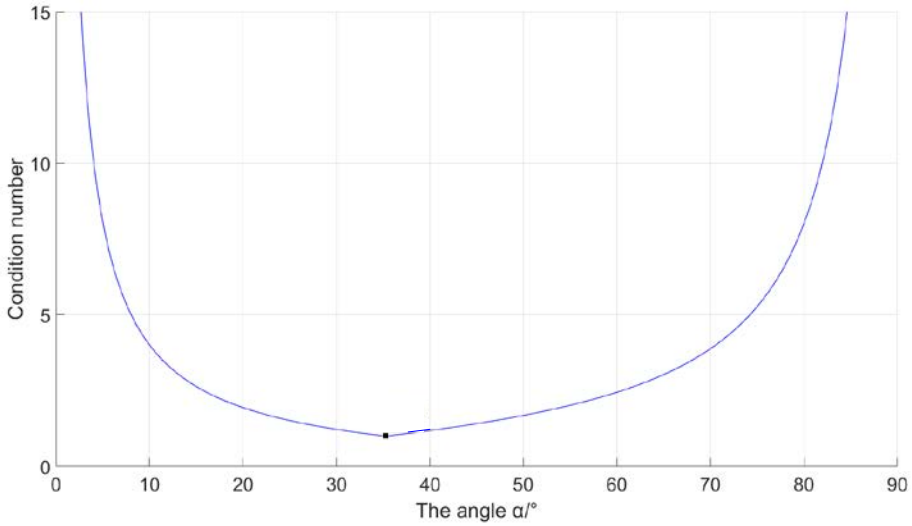


Fig.4 The relationship between the condition number and the tilt angle $\alpha$.

### 3.3.2 The optimization of the reference plane radius

The contour radius of the reference plane is related to measuring space and noninterference space. Based on the theory of displacement sensor, define the maximum of $r_i$ as $r_{max}$, the minimum distance between the probe plane and the sphere surface as $l_{min}$, the axial measurable range of sensor as $\delta$ and the axial vector of sensor $i$ as $\boldsymbol{V}_i$.

During measurement, the sphere center should be limited in the detection space enclosed by one cylinder (the axis coincides with the axis of sensor) and two parallel planes (the planes are perpendicular to the cylinder axis). The distances between the planes and sphere center are $R+l_{min}$ and $R+\delta+l_{min}$ respectively, as shown in Fig.5.

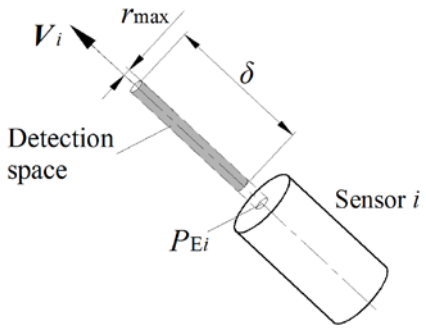


Fig.5 The detection space of sensor $i$.

The measuring space of non-contact R-test is limited in the intersection of detection spaces of three sensors, and it should be a cube shape which is symmetric with respect to MCS. Define the side length of the measuring space as $K$, and the maximum of $K$ can be expressed in the Eq. (7).

$$K = \frac{\min\left(\delta,\ 2r_{max}\right)}{\sqrt{3}} \quad (7)$$

For different sizes of $\delta$ and $r_{max}$, the measuring space could be divided into two cases.

(1) If $\delta \geq 2r_{max}$, the intersection is a polyhedron which is enclosed by three detection spaces. The measuring space is restricted by $r_{max}$, as shown in Fig.6.

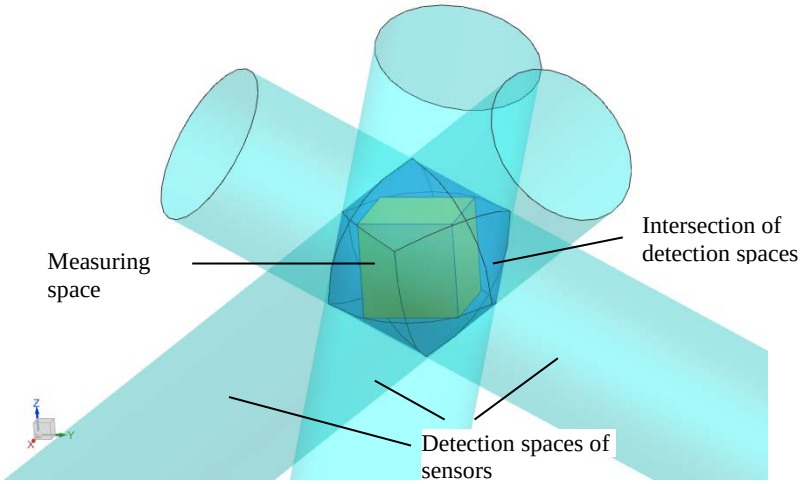


Fig.6 The sketch of detection spaces and measuring space ($\delta \geq 2r_{\max}$).

In order to maximize the noninterference space, the measuring space should be placed as far as possible from the probe plane. Considering the symmetry of measuring space with respect to the MCS, the optimal $\lambda$ could be calculated by solving the Eq.(8).

$$\lambda = \left( \delta + R + l_{\min} - \frac{\sqrt{3}}{2} K \right) \cos\alpha, \text{ if } \delta \geq 2r_{\max} \tag{8}$$

.

(2) If $\delta < 2r_{\max}$, the intersection is a hexahedron which is enclosed by three sets of parallel planes. The measuring space is restricted by $\delta$, as shown in Fig.7.

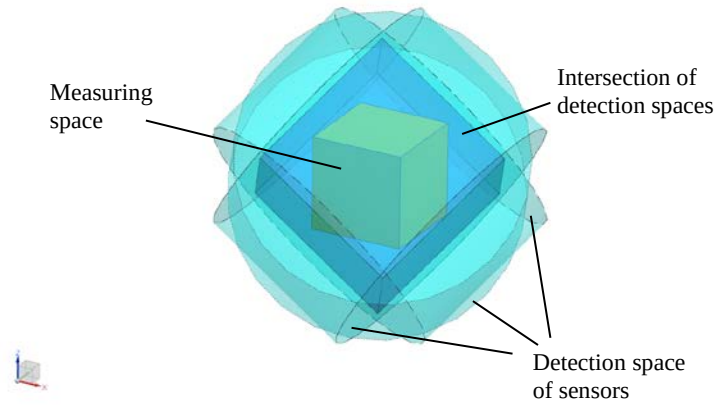


Fig.7 The sketch of detection spaces and the measuring space ($\delta < 2r_{\max}$).

Without loss of generality, suppose the axis of sensor 1 to be located in XOZ coordinate plane of MCS. The measurement constraints for three sensors can be expressed as the Eq. (9) to (11) respectively:

$$\begin{cases} \begin{vmatrix} x-\lambda & y \\ -\lambda & 0 \end{vmatrix}^2 + \begin{vmatrix} y & z+\lambda\cdot\tan\alpha \\ 0 & \lambda\cdot\tan\alpha \end{vmatrix}^2 + \begin{vmatrix} z+\lambda\cdot\tan\alpha & x-\lambda \\ \lambda\cdot\tan\alpha & -\lambda \end{vmatrix}^2 - \left(\lambda^2+\lambda^2\cdot\tan^2\alpha\right)\cdot r_{\max}^2 \le 0, \\ R+l_{\min} \le \dfrac{\left|x-z\cdot\tan\alpha-\lambda-\lambda\cdot\tan^2\alpha\right|}{\sqrt{1+\tan^2\alpha}} \le R+l_{\min}+\delta \end{cases}, \tag{9}$$

$$\begin{cases} \begin{vmatrix} x+\lambda\cdot\sin 30^\circ & y+\lambda\cdot\cos 30^\circ \\ \lambda\cdot\sin 30^\circ & \lambda\cdot\cos 30^\circ \end{vmatrix}^2 + \begin{vmatrix} y+\lambda\cdot\cos 30^\circ & z+\lambda\cdot\tan\alpha \\ \lambda\cdot\cos 30^\circ & \lambda\cdot\tan\alpha \end{vmatrix}^2 + \begin{vmatrix} z+\lambda\cdot\tan\alpha & x+\lambda\cdot\sin 30^\circ \\ \lambda\cdot\tan\alpha & \lambda\cdot\sin 30^\circ \end{vmatrix}^2 \\ -\left(\lambda^2+\lambda^2\cdot\tan^2\alpha\right)\cdot r_{\max}^2 \le 0, \\ R+l_{\min} \le \dfrac{\left|x\cdot\sin 30^\circ+y\cdot\cos 30^\circ+z\cdot\tan\alpha+\lambda+\lambda\cdot\tan^2\alpha\right|}{\sqrt{1+\tan^2\alpha}} \le R+l_{\min}+\delta \end{cases}, \tag{10}$$

$$\begin{cases} \begin{vmatrix} x+\lambda\cdot\sin 30^\circ & y-\lambda\cdot\cos 30^\circ \\ \lambda\cdot\sin 30^\circ & -\lambda\cdot\cos 30^\circ \end{vmatrix}^2 + \begin{vmatrix} y-\lambda\cdot\cos 30^\circ & z+\lambda\cdot\tan\alpha \\ -\lambda\cdot\cos 30^\circ & \lambda\cdot\tan\alpha \end{vmatrix}^2 + \begin{vmatrix} z+\lambda\cdot\tan\alpha & x+\lambda\cdot\sin 30^\circ \\ \lambda\cdot\tan\alpha & \lambda\cdot\sin 30^\circ \end{vmatrix}^2 \\ -\left(\lambda^2+\lambda^2\cdot\tan^2\alpha\right)\cdot r_{\max}^2 \le 0, \\ R+l_{\min} \le \dfrac{\left|x\cdot\sin 30^\circ-y\cdot\cos 30^\circ+z\cdot\tan\alpha+\lambda+\lambda\cdot\tan^2\alpha\right|}{\sqrt{1+\tan^2\alpha}} \le R+l_{\min}+\delta \end{cases}. \tag{11}$$

The larger intersection of detection spaces is, the larger measuring space is. And the measuring space should be placed as far as possible from the probe plane. Define the number of valid sphere centers (which are uniform distributed in the measuring space) as $S$. In order to obtain the optimal $\lambda$ to maximize the measuring space and noninterference space, the algorithm of Monte Carlo is applied to establish the relationship between $S$ and $\lambda$. The optimization process can be described as follows:

Step 1: Divide the intersection of detection spaces into equal parts by interval $e_0$ to obtain uniformly distributed points set of $P_j$ ($j$=1, 2, …, $n$);

Step 2: Divide $\lambda$ into equal segments by interval $\lambda_0$ to obtain sequence items of $\lambda_k$ ($k$=1, 2, … , $m$);

Step 3: Set the initial $S$ to 0, and input $r_{\max}$, $r$, $R$, $l_{\min}$, $\delta$, $\alpha$, $\lambda_k$ and $P_j$ into the Eq. (9) to (11);

Step 4: If the Eq. (9) to (11) are satisfied, it indicates that point $P_j$ is in the measuring space, $S$=$S$+1, otherwise $P_j$ is out of it.

Step 5: Update $\lambda_k$, and go to step 4 until the sequence item reaches the end;

Step 6: The optimal $\lambda$ is the $\lambda_k$ which is corresponding to the maximum of $S$.

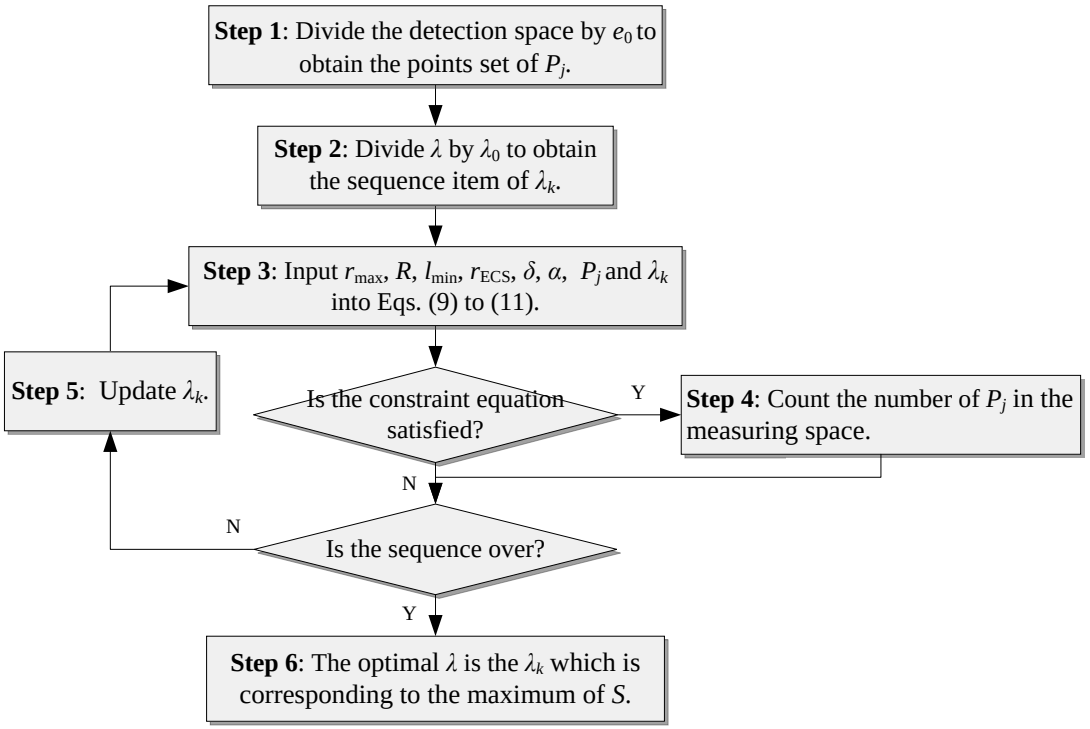


Fig.8 The optimization process for the reference plane radius.

## 3.4 The on-machine calibration

According to normal regulations, non-contact R-test is pre-calibrated by manufacturer periodically to reduce assembly errors and sensor errors, which are costly for manufacture and maintenance. In addition, before measurement, it is necessary to ensure the consistency of MCS and machine coordinate system with re-calibration by user[17]. This would result in a lot of time, effort and cost. Typical positioning error of linear axis is less than 0.1 μm/1 mm, and typical measuring space is only about 1 $mm^3$. So, the re-calibration can be accomplished by the positioning movement of the machine tool to be tested. For the re-calibration of IBS, the sphere is controlled to be moved/stepped about 0.2 mm relative to the fixture in the X/Y/Z axes of the machine coordinate system. And then, the MCS is aligned to the machine coordinate system by corresponding rotation matrix[9].

However, even if the precision of pre-calibration is high, the final measurement accuracy could be influenced to a great degree by re-calibration. So, on-machine calibration is feasible to replace the pre-calibration and re-calibration before measurement by user.

### 3.4.1 The definition of theoretic MCS

The fixture can be placed on the worktable at any position based on the requirement of measurement. By controlling the linear axes of the machine tool, the sphere center is located approximately at the intersection of sensors axes. Then the sphere center is defined as the origin of theoretic MCS which can be recorded by sensors reading, and the axes of theoretic MCS are defined to parallel to the corresponding axes of machine coordinate system.

### 3.4.2 The registration of actual MCS

According to the structure and measurement principles of non-contact R-test, the actual MCS is defined by the postures of sensors fixed by the fixture installed on worktable. So the on-machine calibration is converted to the registration from ideal MCS to actual one. It can be realized by the solution for the parameters of probe planes based on the actual MCS.

By controlling linear axes of the machine tool, the sphere center is located at any 12 points $P_j(x_j, y_j, z_j)$ ($j$=1,...,12) based on the ideal MCS in the measuring space. The registration can be regarded as an inverse operation of the calculation of the sphere center coordinates. The coordinates of point $P_j$ are applied as known quantity to the Eq. (2), then the parameters of a probe plane about $a_i$, $b_i$, $c_i$, $d_i$ and $P_{Ei}$ based on the actual MCS can be solved.

## 3.5 The prediction of measurement accuracy

### 3.5.1 The analysis of calibration error

For the on-machine calibration, the calibration error $\Delta_{ca}$ can be defined as the origin deviation of actual MCS from ideal one. In calibration process, some errors may be introduced (e.g. the positioning error $\Delta p$ of the machine tool, the contour error $\Delta R$ of the sphere).

Define the actual center of probe plane $i$ in ideal MCS as $P'_{Ei}(x'_{Ei}, y'_{Ei}, z'_{Ei})$. The relationship about $P'_{Ei}$ and above errors can be expressed as follows:

$$\begin{aligned} & f_j\left(a_i, b_i, c_i, d_i, x'_{Ei}, y'_{Ei}, z'_{Ei}\right) \\ & =\left(\left(x_j+\Delta p\right)-x'_{Ei}\right)^2+\left(\left(y_j+\Delta p\right)-y'_{Ei}\right)^2+\left(\left(z_j+\Delta p\right)-z'_{Ei}\right)^2-r_i^2-\left(L_i+\Delta R\right)^2=0, \quad (i=1,2,3, \quad j=1,\ldots,12) \end{aligned} . \tag{12}$$

According to the Eq. (12), the calibration error $\Delta_{ca}$ can be analyzed:

$$\Delta_{ca}=\left\|\left(\frac{\sum_i^3\left(x'_{Ei}-x_{Ei}\right)}{3} \quad \frac{\sum_i^3\left(y'_{Ei}-y_{Ei}\right)}{3} \quad \frac{\sum_i^3\left(z'_{Ei}-z_{Ei}\right)}{3}\right)\right\|, \quad (i=1,2,3). \tag{13}$$

The relationship between the positioning error of the machine tool and the calibration error is shown in Fig.9.

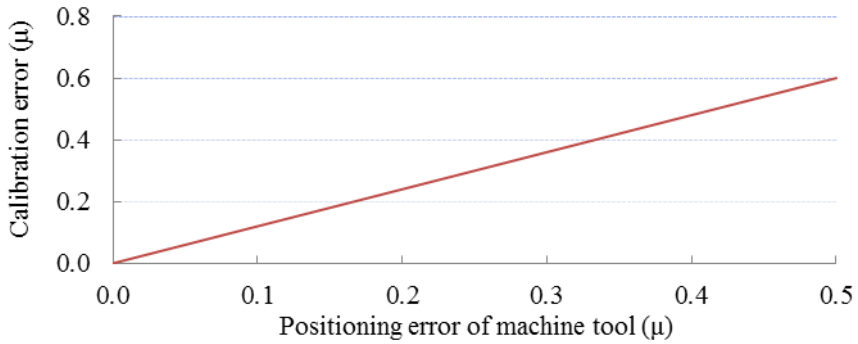


Fig.9 The relation between the positioning error of the machine tool and the calibration error.

### 3.5.2 The prediction of measurement error

In measurement process, some errors may be introduced into the finial result (e.g. the sensor error $\Delta l$,

contour error $\Delta R$, and calibration error $\Delta_{ca}$). According to the Eq. (3), the relationship about the actual coordinates of point $P$ ($x'$, $y'$, $z'$) and the above errors can be expressed as follows:

$$f_i(x',y',z')=(x'-x'_{Ei})^2+(y'-y'_{Ei})^2+(z'-z'_{Ei})^2-r_i^2-(L_i+\Delta l+\Delta R)^2=0,\quad (i=1,2,3), \tag{14}$$

According to the Eq. (14), the measurement error can be predicted as follows:

$$\Delta=\left|\begin{pmatrix}(x'-x) & (y'-y) & (z'-z)\end{pmatrix}\right|. \tag{15}$$

The relationships of the calibration error, sensor error and measurement error of R-test are shown in Fig.10 and Fig.11.

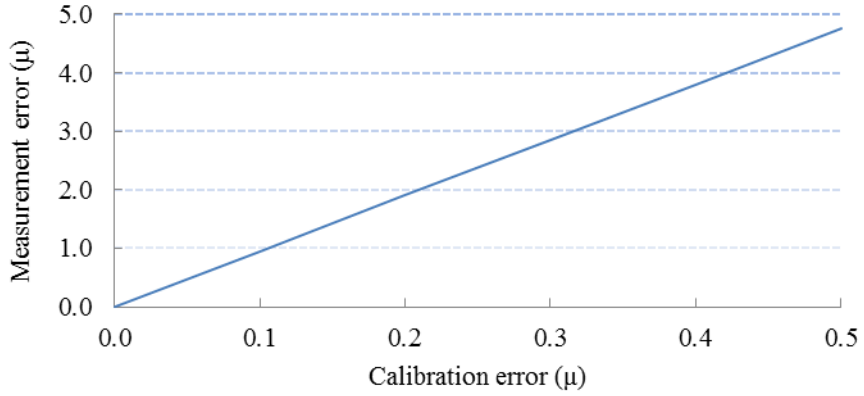


Fig.10 The relation between the measurement error and calibration error.

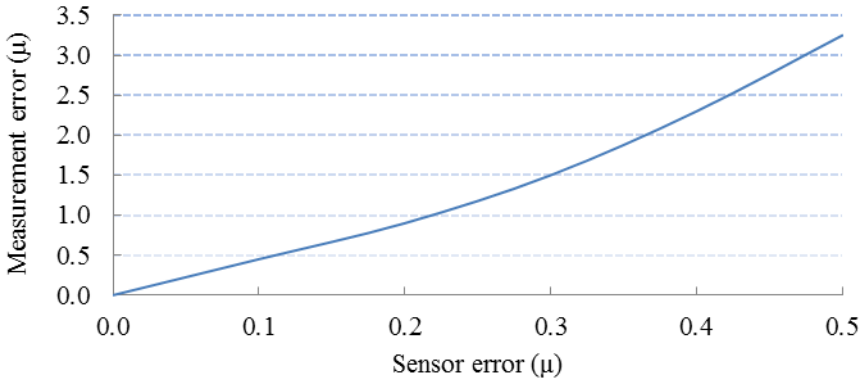


Fig.11 The relation between the measurement error and sensor error.

## 3.6 Judgment of iterative optimization

According to the above analysis, the higher precision of the sensor, sphere and on-machine calibration, the higher measurement accuracy can be achieved. The optimization goal of structural parameters is to improve the measurement stability, measuring space and noninterference space. The calibration error can be controlled below 0.1 μm by laser interferometer. So the iterative optimizations are related to the adjustment of the sensor and sphere parameters to achieve the balance between minimum cost and definite accuracy.

Non-contact displacement sensor has different types, such as eddy current sensor (ECS), capacitive sensor, laser displacement sensor and so on. The main differences of them are measurement accuracy,

sampling frequency and requirement for application environment. In addition, cost, availability, stability, capability etc. should be considered comprehensively.

In order to reasonably determine the parameters, the relationship between the cost and measurement accuracy is researched. Define the cost for $\Delta R$ as $f(\Delta R)$, the cost for $\Delta l$ as $f(\Delta l)$. The total cost of non-contact R-test can be expressed as follows:

$$\text{cost} = f(\Delta R) + f(\Delta l) + F, \tag{16}$$

where $F$ is the other fixed cost.

When the total cost is limited in a certain range, the minimum of total cost could be used to calculate the performances of the sensor and sphere by the Eq. (7) to (15). If the solution fails, the cost will be raised for iterative calculation until the maximum cost is reached. If the solution still cannot be satisfied, it means that the measurement accuracy cannot be satisfied under the cost requirement.

# 4 Application and verification

## 4.1 Description of case study

A prototype was developed to verify the proposed method. In order to meet the measurement requirements of most machine tools, the measuring space is set to 1 $mm^3$ based on MCS and the maximum measurement error is set to 5 μm.

### 4.1.1 The structure parameters

The sphere is made of steel and diameter is 30 mm, of which contour error is less than 0.1 μm. It is fixed at the end of a special holder which can adjust the sphere position in radial direction.

Relative to other sensors, ECS has advantages of high precision and resolution, high temperature stability, high response frequency up to 100 kHz[27]. According to the diameter of the sphere, measurable range, cost and accuracy, the ECS of Kaman KD-2306 6U1 ( $r$ is 7.1 mm, $\delta$ is 6 mm, $l_{\min}$ is 0.2 mm, resolution is 0.6 μm, frequency response is 50 kHz) is selected for the prototype. In addition, because eddy current induced in the sphere is related to the electrical conductivity and magnetic permeability of material attributes (e.g. crystal structure, chemical composition, surface treatments, residual magnetic field), a special coating for the sphere is considered.

According to the Eq. (7) to (11), $\lambda$ is set to 16.601 mm. The noninterference projected area of sphere center in XOY coordinate plane is about 134.092 $mm^2$.

ECS represents the distance between the sphere center and the probe plane by induced voltage. Define the induced voltage of the ECS $i$ as $U_i$. In order to describe the inductive effect more accurately, polynomial fitting is used to express the conversion from $U_i$ to $L_i$ (It can be obtained by sensor calibration[28], and the sensor error $\Delta l$ is less than 0.1 μm/1.8 mm).

$$\begin{cases} U_1 = 0.532L_1^{0.5} + 0.065r_1^{0.5} + 0.168, \\ U_2 = 0.526L_2^{0.5} + 0.072r_2^{0.5} + 0.183, \\ U_3 = 0.531L_3^{0.5} + 0.068r_3^{0.5} + 0.168, \\ 21.2 - \sqrt{3} \le L_{1,2,3} \le 21.2, \end{cases} . \tag{17}$$

The interference of eddy current is generated with each other when sensors are energized simultaneously. Since the sensors work at the same frequency and the mutual distance is less than two sensor diameter for the prototype, the interference could cause significant sensor error. In order to eliminate the interference, time-sharing and synchronized circuits were considered[28].

Fig.12 The prototype of non-contact R-test.

### 4.1.2 The on-machine calibration

A series of on-machine calibration experiments were conducted on a five-axis machine tool of DMG DMU 100 mono BLOCK. The positioning error of X/Y/Z axes about 0.1 μm/1 mm was calibrated by laser interferometer of Renishaw XL-30, as shown in Fig.13(a).

(a) Positioning calibration. (b) Actual MCS calibration.

Fig.13 The scene of on-machine calibration process.

According to the parameters of the sensor and the fixture structure, the induced voltage is set to 2.561 V when the sphere center is at the origin of ideal MCS. Then X/Y/Z axes of the machine tool were controlled to locate the sphere center at 12 calibration points, as shown in Fig. 13(b). The results of on-machine calibration are shown in Tab.2 and Tab.3.

Tab.2 The coordinates of calibration points and the corresponding induced voltages.

| Calibration point | Ideal coordinates (mm) | | | Induced voltage (V) | | |
|---|---|---|---|---|---|---|
| | $x$ | $y$ | $z$ | $U_1$ | $U_2$ | $U_3$ |
| $P_1$ | -0.282 | 0.138 | -0.260 | 2.6133 | 2.5874 | 2.5725 |
| $P_2$ | 0.038 | -0.434 | -0.092 | 2.6025 | 2.5751 | 2.6188 |
| $P_3$ | -0.255 | 0.081 | 0.482 | 2.6282 | 2.6184 | 2.6202 |
| $P_4$ | -0.465 | 0.439 | 0.161 | 2.6389 | 2.6223 | 2.5893 |
| $P_5$ | -0.316 | -0.481 | -0.039 | 2.6263 | 2.5647 | 2.6250 |
| $P_6$ | 0.307 | -0.037 | -0.326 | 2.5601 | 2.5991 | 2.6044 |
| $P_7$ | -0.267 | 0.473 | 0.192 | 2.6318 | 2.6229 | 2.5902 |
| $P_8$ | 0.059 | 0.245 | 0.209 | 2.6088 | 2.5957 | 2.5992 |
| $P_9$ | -0.255 | 0.289 | 0.499 | 2.6363 | 2.6276 | 2.6162 |
| $P_{10}$ | 0.360 | 0.199 | 0.132 | 2.5953 | 2.6097 | 2.6103 |
| $P_{11}$ | -0.314 | 0.458 | 0.048 | 2.6297 | 2.6181 | 2.5794 |
| $P_{12}$ | 0.166 | -0.392 | 0.246 | 2.6111 | 2.6024 | 2.6070 |

Tab.3 The parameters of probe planes based on actual MCS.

| Plane | $a_i$ | $b_i$ | $c_i$ | $d_i$ | $x_{Ei}$ | $y_{Ei}$ | $z_{Ei}$ |
|---|---|---|---|---|---|---|---|
| 1 | -0.2692 | 0.0269 | 0.1913 | 6.7382 | 16.5205 | -1.6510 | -11.7396 |
| 2 | 0.1230 | 0.1780 | 0.1481 | 5.3315 | -9.5400 | -13.8008 | -11.4889 |
| 3 | 0.0864 | -0.1823 | 0.1473 | 5.0788 | -7.0345 | 14.8396 | -11.9905 |

Through the above analysis, the calibration error is predicted about 0.25 μm. Considering the sensor error and contour error of the sphere, the measurement error of the prototype is predicted about 3.5 μm.

## 4.2 The verification of measurement accuracy

To verify the measurement accuracy of the prototype, three different points of the sphere center in measuring space were selected. Following the same operation, the corresponding inducted voltages were obtained, as shown in Tab.4.

Tab.4 The induced voltages of sphere center (unit: V) .

| Point | $U_1$ | $U_2$ | $U_3$ |
|---|---|---|---|
| $P_1$ | 2.5968 | 2.6115 | 2.5678 |
| $P_2$ | 2.5886 | 2.6139 | 2.5885 |
| $P_3$ | 2.6130 | 2.5888 | 2.5705 |

According to the solution of the sphere center coordinates, the results of measurement error are shown in Tab.5. The maximum measurement error is about 3.1 μm, which is in the predicted range.

Tab.5 The comparison result of measurement error (unit: mm).

| Point | Actual coordinates | | | Ideal coordinates | | | Error |
|---|---|---|---|---|---|---|---|
| | $x'$ | $y'$ | $z'$ | $x$ | $y$ | $z$ | |
| $P_1$ | 0.0581 | 0.3691 | -0.4942 | 0.058 | 0.369 | -0.496 | 0.0018 |
| $P_2$ | 0.256 | 0.332 | -0.1879 | 0.256 | 0.332 | -0.189 | 0.0011 |
| $P_3$ | -0.2719 | 0.158 | -0.2701 | -0.273 | 0.156 | -0.268 | 0.0031 |

## 4.3 The verification of measurement accuracy

To verify the measurement accuracy of the prototype, some tests based on ISO 230-7 and ISO 10791-6-BK1 were performed. The distance between C-axis and the origin of MCS was set to 200 mm. To improve measurement stability, the test began after the machine had run for 1 hour. All data were measured three times in single direction. It can reduce the error caused by machine thermal deformation, lubricating inadequacy, moving clearance and so on.

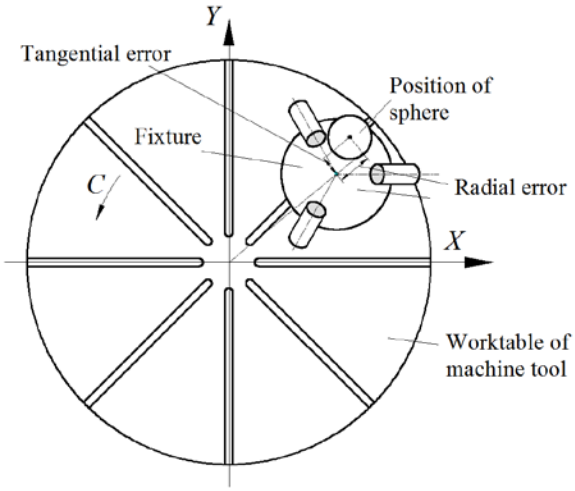


Fig.14 The synchronous errors with simultaneous C/X/Y axes interpolation.

For static test, the C-axis was commanded to rotate from 0 to 360˚, which was divided to 36 equal divisions: C=0˚, 10˚, …. 350˚, 360˚. The RPCP function of the machine tool was active, and the sphere was commanded to follow the fixture in X/Y axes (federate is 5000 mm/min). The interpolation was suspended for 4 seconds in each interval, and the prototype measured static synchronous errors in radial, tangential and axial directions automatically. Moreover, a DBB of Renishaw QC10 was conducted to verify the accuracy of prototype[29], as shown in Fig.15. The comparisons of measurement results are shown in Fig.16.

(a) In radial direction. (b) In tangential direction. (c) In axial direction.

Fig.15 Measurement scene with DBB.

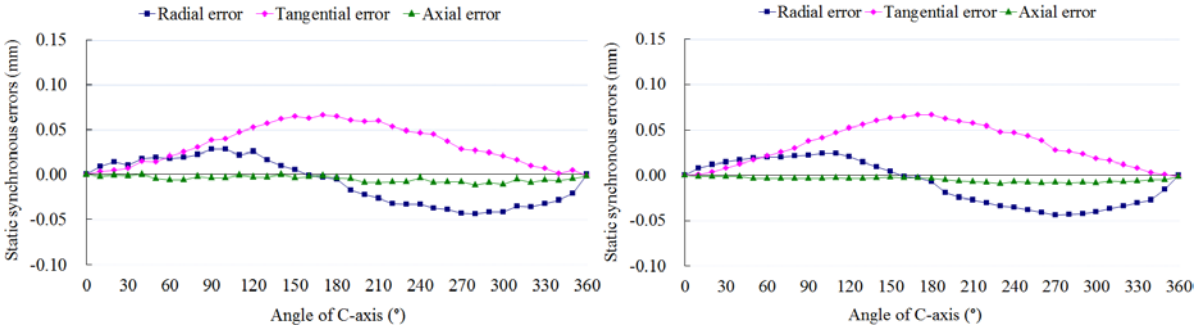


(a) With prototype. (b) With DBB.

Fig.16 The comparisons of measurement results for static test.

For dynamic test, the C-axis was commanded to rotate from 0 to 360˚ with a constant angular velocity. The RPCP was active, and the sphere was commanded to follow the fixture in X/Y axes (the feedrate is 5000 mm/min). The prototype continuously measured synchronous errors at 1 kHz automatically. Similar to the previous method, a DBB was conducted. The comparisons of radial, tangential and axial measurement results are shown in Fig.17 to Fig.19.

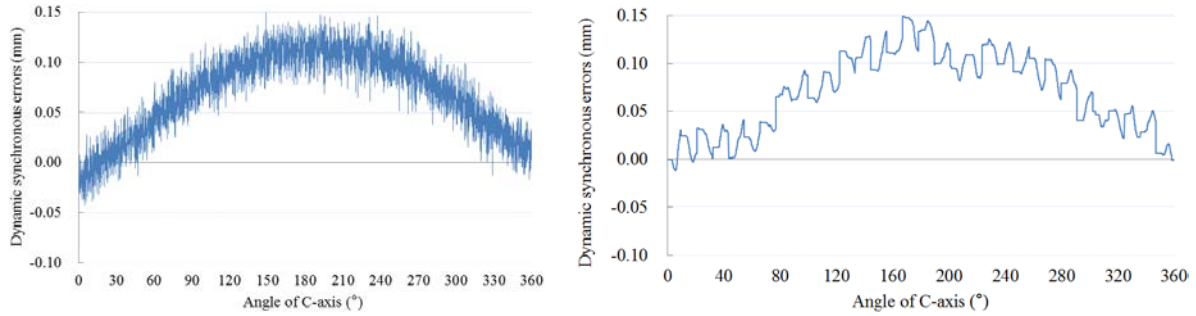


(a) With prototype. (b) With DBB.

Fig.17 The comparison of measurement results for dynamic test (radial).

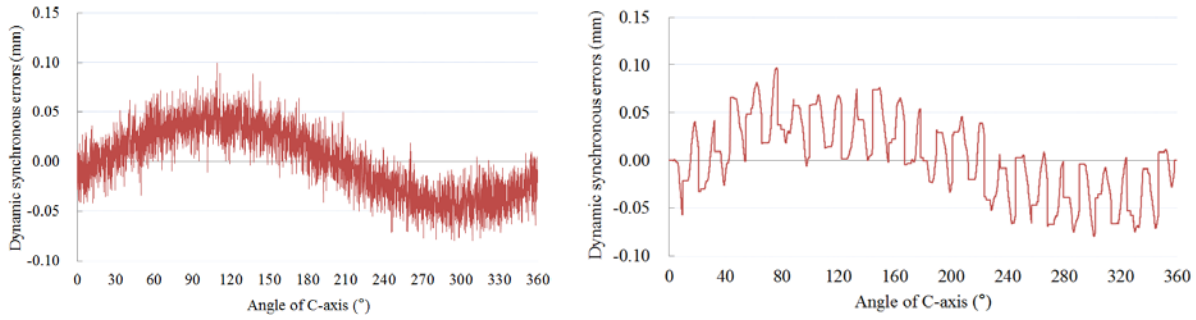


(a) With prototype. (b) With DBB.

Fig.18 The comparison of measurement results for dynamic test (tangential).

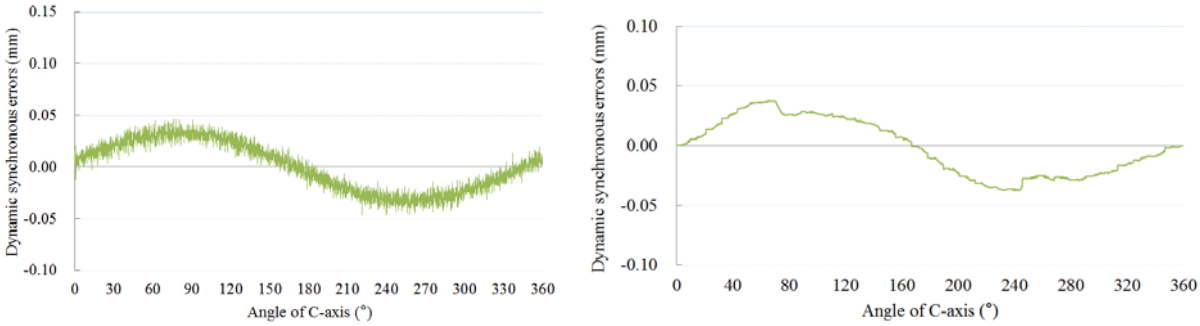


(a) With prototype. (b) With DBB.

Fig.19 The comparison of measurement results for dynamic test (axial).

The measurement results (data and trends) of the prototype and DBB have good consistency, which proves that the proposed optimization method is effective for non-contact R-test.

# 5 Conclusion

In this paper, a systematic optimization method for improving non-contact R-test accuracy is proposed. Its problem spaces and controls are explored and the overall flowchart of the optimization process is advised and tested. The results indicate that:

(1) The proposed optimization method can improve measurement accuracy iteratively by the parameters optimization of the fixture structure, the on-machine calibration, the prediction of measurement accuracy and the adjustment of the sensor and sphere parameters.

(2) The calculation of the sphere center coordinates based on SADE algorithm can obtain the definite computational accuracy and efficiency.

(3) The parameters optimization of the fixture structure can maximize the performances of measurement stability, measuring space and noninterference space.

(4) The on-machine calibration replaces pre-calibration and re-calibration to establish the positional relationships between sensors, the fixture and the machine tool to be tested simultaneously. It can reduce the difficulties for manufacture, maintenance and use.

(5) The prediction of measurement accuracy can help select appropriate components with a good balance between the minimum cost and measurement accuracy.

Through a series of static and dynamic tests, it is verified that the proposed method is effective, which could be applied for further development of non-contact R-test.

## Acknowledgements

This work is supported by the intelligent manufacturing fund of the New Mode Application of Intelligent Manufacturing for the Key Components of High Speed Emu (2016ZNZZ01-05), from the ministry of industry and information technology, China.

## Appendix

Notation

| Parameter | Meaning |
|---|---|
| $a_i$, $b_i$, $c_i$, $d_i$ | The ideal parameters of probe plane $i$. |
| $e_0$ | The unit interval of measurable search range. |
| $i$ | The serial number of sensor. |
| $j$ | The serial number of calibration points. |
| $\boldsymbol{J}$ | The relationship matrix of the sphere center coordinates and $L_{i\text{-}j}$. |
| $K$ | The side length of measuring space |
| $l_i$ | The distance between the probe plane $i$ and sphere surface. |
| $l_{\min}$ | The minimum distance between the probe plane and sphere surface. |
| $L_i$ | The distance between the probe plane $i$ and sphere center. |
| $n$ | The total number of the possible measuring space divisions of R-test. |
| $P$ | The point of sphere center. |
| $P_{Ei}$ | The ideal center point of probe plane $i$. |
| $P'_{Ei}$ | The actual center point of probe plane $i$. |
| $P_j$ | The $j$-th calibration points. |
| $r_i$ | The distance between the axis of sensor $i$ and sphere center. |
| $r_{\max}$ | The maximum of sphere center radially deviation from the sensor axis. |
| $R$ | The radius of sphere. |
| $r$ | The radius of probe plane. |
| $S$ | The number of sphere center which is in the measuring space. |
| $\boldsymbol{V}_i$ | The axis vector of sensor $i$. |
| $U_i$ | The induced voltage of ECS $i$. |
| $(x, y, z)$ | The ideal coordinates of point $P$. |
| $(x', y', z')$ | The actual coordinates of point $P$. |
| $(x_j, y_j, z_j)$ | The coordinates of point $P_j$. |
| $(x_{Ei}, y_{Ei}, z_{Ei})$ | The coordinates of point $P_{Ei}$. |
| $(x'_{Ei}, y'_{Ei}, z'_{Ei})$ | The coordinates of point $P'_{Ei}$. |

| | |
|---|---|
| $\alpha$ | The tilt angle between the axis of sensor and reference plane. |
| $\delta$ | The measurable range of sensor. |
| $\lambda$ | The contour radius of reference plane. |
| $\lambda_0$ | The interval of $\lambda$ sequence. |
| $\lambda_k$ | The sequence item of $\lambda$. |
| $\Delta l$ | The sensor error. |
| $\Delta R$ | The contour error of sphere. |
| $\Delta p$ | The positioning error $\Delta p$ of machine tool. |
| $\Delta$ | The measurement error. |
| $\Delta_{ca}$ | The calibration error. |

# References


[1] Lei Z, Qingzhen B, Nuodi H, Yuhan W. Dynamic accuracy evaluation for five-axis machine tools using S trajectory deviation based on R-test measurement[J]. International Journal of Machine Tools and Manufacture, 2018, 125: 20-33.

[2] Hong C., Ibaraki S. Non-contact R-test with laser displacement sensors for error calibration of five-axis machine tools[J]. Precision Engineering, 2013, 37(1): 159-171.

[3] Weikert S. R-Test, A new device for accuracy measurements on five axis machine tools[J]. CIRP Annals-Manufacturing Technology, 2004, 53(1): 429-432.

[4] ISO 230-1:2012, Test code for machine tools - Part 1: Geometric accuracy of machines operating under no-load or quasi-static conditions; 2012.

[5] ISO 230-7: Test code for machine tools - Part 7: Geometric accuracy of axes of rotation, International Organization for Standardization (ISO), Geneva, Switzerland, 2015.

[6] ISO 10791-6: Machine Tools - Test conditions for machining centres Part 6: Accuracy of speeds and interpolations, International Organization for Standardization (ISO), Geneva, Switzerland, 2014.

[7] Hong C., Ibaraki S., Matsubara A. Influence of position-dependent geometric errors of rotary axes on a machining test of cone frustum by five-axis machine tools[J]. Precision Engineering, 2011, 35: 1-11.

[8] Liu D. W., Guo Z. P., Song Z. Y. An optimum structural design method of r-test ball sphere center measuring device[J]. Journal of Mechanical Engineering, 2013, 49(23): 161-166.

[9] Rotary analyzer user’s manual, IBS Precision Engineering BV, Eindhoven, Netherlands, 2016.

[10] Machine tool inspection & analyzer solutions, IBS Precision Engineering BV, Eindhoven, Netherlands, 2018.

[11] HMS (Head Measuring System), FIDIA S.p.A, San Mauro Torinese, Italy, 2018.

[12] Li L. L., Du Z. C. Model analysis of a novel error measurement device of five-axis manufacturing center[J]. Journal of Shanghai Jiao Tong University. 2013,47(11): 1801-1806.

[13] Bringmann B., Knapp W. Model-based 'Chase-the-Ball' calibration of a 5-axes machining center[J]. CIRP Annals-Manufacturing Technology, 2006, 55(1): 531-534.

[14] Hong C., Ibaraki S., Oyama C. Graphical presentation of error motions of rotary axes on a five-axis

machine tool by static R-test with separating the influence of squareness errors of linear axes[J]. International Journal of Machine Tools & Manufacture, 2012, 59: 24-33.
[15] Ibaraki S, Oyama C, Otsubo H. Construction of an error map of rotary axes on a five-axis machining center by static R-test[J]. International Journal of Machine Tools and Manufacture, 2011, 51(3): 190-200.
[16] Bringmann B, Maglie P. A method for direct evaluation of the dynamic 3D path accuracy of NC machine tools[J]. CIRP Annals - Manufacturing Technology, 2009; 58(1): 343-6.
[17] Ota Y, Ibaraki S. Evaluation of dynamic errors of rotary axis in five-axis machining centers at the reversing point[C]. Proceedings of the Mechanical Engineering Congress, ASME, 2011.
[18] ISO/TR 17243-2:2017: Machine tool spindles - evaluation of spindle vibrations by measurements on non-rotating parts - Part 2: Direct-driven spindles and belt-driven spindles with rolling element bearings operating at speeds between 600 r/min and 30 000 r/min, International Organization for Standardization (ISO), Geneva, Switzerland, 2017.
[19] Li J., Xie F. G., Li W. D. A geometric error identification method for the swiveling axes of five-axis machine tools by static R-test[J]. International Journal of Advanced Manufacturing Technology, 2017, 89(9-12): 3393-3405.
[20] Florussen G. H. J., Spaan H. A. M. Dynamic R-Test for rotary tables on 5-axes machine tools[C]. Procedia CIRP, 2012, 1: 536-539.
[21] Spaan H. A. M., Florussen G. H. J. Determining the 5-axes machine tool contouring performance with dynamic R-test measurements[C]. Proceedings of the 12th Euspen International Conference, 2012.
[22] Florussen, G. H. J., Morel M. A. A., Spaan H. A. M. Assessing the impact of rotary axes on the dynamic accuracy of machine tools[C]. Lamdamap conference IX, Brunel University, UK, 2009.
[23] Ihara Y, Hiramatsu Y. Design of motion accuracy measurement device for NC machine tools with three displacement sensors[J]. International Journal of Automation Technology, 2011, 5(6): 847-54.
[24] Tasoulis D. K., Pavlidis N. G., Plagianakos V. P., et al. Parallel Differential Evolution. Evolutionary Computation, 2004, 2: 2023-2029.
[25] Storn R, Price K (1997) Differential Evolution - A simple and efficient heuristic for global optimization over continuous spaces. Journal of Global Optimization 11(4):341-359.
[26] Lei J, Yong L, Yisheng Z, et al. Posture adjustment of workpiece based on stepwise matching by self-adaptive differential evolution algorithm[J]. Mechanical Sciences, 2018, 9: 267-276.
[27] Eddy current sensors for displacement and position, MICRO-EPSILON Headquarters, Ortenburg, Germany, 2017.
[28] KD-2306 non-contact displacement measuring system user’s manual, Kaman Precision Products, Middletown, the United States of America, 2009.
[29] Lei J, Guofu D, Zhuang L, et al. Geometric error model and measuring method based on worktable for five-axis machine tools[J]. Proceedings of the Institution of Mechanical Engineers, Part B: Journal of Engineering Manufacture, 2013, 227(1):32-44.